

# 3-Dimensional Hydrothermal Vent Localization Based on Chemical Plume Tracing

Lingxiao Wang

*Dept. of Electrical Engineering  
and Computer Science  
Embry-Riddle Aeronautical University  
Daytona Beach, FL, 32114  
lingxiaw@my.erau.edu*

Shuo Pang

*Dept. of Electrical Engineering  
and Computer Science  
Embry-Riddle Aeronautical University  
Daytona Beach, FL, 32114  
shuo.pang@erau.edu*

Guangyu Xu

*Acoustics Department  
University of Washington  
Applied Physics Laboratory  
Seattle, WA, 98115  
guangyux@apl.uw.edu*

**Abstract**—This paper presents a 3-dimensional (3-D) chemical plume tracing (CPT) algorithm for using on an autonomous underwater vehicle (AUV) to find a hydrothermal vent in the underwater environment. In the process of tracing hydrothermal plumes, two types of search modes are defined, namely the horizontal and the vertical search mode. Specifically, in the horizontal search mode, the AUV employs the moth-inspired CPT method to trace plumes on a horizontal plane, and when the vertical search mode is activated, the AUV follows 3-D spiral trajectories to detect plumes in deeper water regions. These two search modes are alternated until the hydrothermal vent is located. In experiments, a 3-D hydrothermal plume simulator, which was created based on the plume data collected from real active vents, is employed as the simulation environment. Results from simulation tests verify that the proposed CPT algorithm is valid for locating a hydrothermal vent in a 3-D underwater environment.

**Index Terms**—Hydrothermal vent localization, Chemical plume tracing, Hydrothermal plume simulation

## I. INTRODUCTION

Hydrothermal vents are essential to the global ocean chemistry. They serve as natural plumbing systems that transport heat and minerals from the interior of the Earth to the ocean and also support complex and unique ecosystems that are valuable for people to study the evolution of life on Earth [1]. To locate an active hydrothermal vent, surveying hydrothermal plumes is the most effective approach. The emitted hydrothermal plumes are physically and chemically distinct from surrounding seawater and disperse following a spatial trajectory largely driven by ocean currents [2]. Historically, hydrothermal vent discovery was mainly performed by human-occupied submarine vehicles or tethered sensor networks, which are limited by surface conditions and low search efficiencies [3]. In recent years, employing autonomous underwater vehicles (AUVs) for marine surveys has become more and more popular [4], and several successful AUV-based hydrothermal vent discovery have been demonstrated during expeditions in both the Pacific [5] and the Atlantic Oceans [6]. However, one aspect of AUVs that was not fully studied during these expeditions is their capacity for autonomous hydrothermal plume tracing, which is referred to as the problem of chemical plume tracing (CPT) [7].

The challenging part of designing an effective CPT algorithm is estimating the locations of hydrothermal plumes and letting the AUV continuously detect plumes. In laminar flows, plume dispersal is mainly due to advection and molecular diffusion, which results in a spatially coherent trajectory [8]. In turbulent flows, hydrothermal plumes are stretched and twisted, which results in an intermittent and patch plume trajectory. The intuitive chemotaxis CPT algorithm [9], which traces plumes by following the concentration gradient, is not practical in turbulent flow environments.

Alternatively, the bio-inspired and engineering-based CPT methods are proposed to solve this problem. A bio-inspired method designs a CPT algorithm by mimicking animal olfactory behaviors. For instance, inspired by the mate-seeking behaviors of male moths, which could find a female moth by tracking the emitted pheromone plumes over a long distance [10], the moth-inspired CPT algorithm is proposed [11]. By contrast, engineering-based CPT methods utilize mathematical and physics-based approaches to estimate plume distributions and possible hydrothermal vent locations, such as Bayesian inference [12], particle filter [13], hidden Markov model (HMM) [14], and partially observable Markov decision process (POMDP) [15]. After the AUV obtains the estimated vent location, a searching trajectory that leads the AUV to move toward the target will be generated via path planners. For instance, the artificial potential field (APF) [16] and A-star [17] path planning algorithms are suitable methods to produce searching trajectories. Besides, Vergassola et al. proposed the 'infotaxis' method [18], which uses the information entropy to guide a plume-tracing robot. The robot is commanded to move toward the direction that reduces the information uncertainty.

Fig. 1 presents the structure of the emitted hydrothermal plumes, which comprises two components, namely buoyant and non-buoyant plumes. Emitted hydrothermal plumes rise vigorously in a column above the vent and form buoyant plumes. Then, the rising hydrothermal plumes are continuously diluted by the ambient water. After reaching neutral buoyancy, diluted plumes expand horizontally and turn into the non-buoyant plumes. Dimensions of the non-buoyant plumes could range from tens to hundreds of kilometers at approximately hundreds of meters above the seafloor [19].

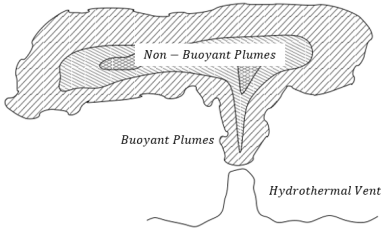


Fig. 1. Demonstration of the structure of a hydrothermal plume. The buoyant and non-buoyant components inside a hydrothermal plume are labeled.

Due to the complexity of a 3-dimensional (3-D) hydrothermal vent localization problem, most published CPT algorithms simplified this problem in a 2-D plane, in which the AUV is targeted to find the hydrothermal vent location on a horizontal cross-section of a non-buoyant plume (e.g., [20]–[22]). However, it can be seen from Fig. 1 that in real circumstances, hydrothermal plumes disperse in a 3-D space instead of a 2-D plane. Thus, designing a CPT algorithm that traces and finds hydrothermal vents in 3-D environments is more suitable for real-world applications.

A 3-D CPT algorithm for locating hydrothermal vents using AUVs is proposed in this paper. During the process of tracing hydrothermal plumes, two types of search modes, i.e., horizontal and vertical search modes, are defined. Specifically, the AUV adopts the moth-inspired CPT algorithm [11] to trace plumes in the horizontal search mode, and if the AUV has not detected plumes for a long time (i.e., the non-detection period exceeds a specified threshold), it switches to the vertical search mode. Then, 3-D spiral searching trajectories that lead the AUV to find plumes in the deeper water regions are calculated based on the AUV current position. If the plume non-detection period is beyond the limit, the AUV switches back to the horizontal search mode. These two search modes are alternated until the AUV reaches the minimal altitude, and the localization task is treated as complete if the AUV finds the hydrothermal vent location within the maximal time limit (the declaration of the vent location could be done with aids of external sensors, such as onboard cameras, which could recognize the hydrothermal vent appearance to determine whether a vent is located), and if the running time is beyond the maximal time limit, the localization task is terminated and the AUV returns to the initial position.

## II. METHODOLOGY

### A. The Framework of the Proposed CPT Method

Fig. 2 shows the framework of the proposed CPT method. The AUV starts the searching process in the horizontal mode, while the plume non-detection period  $\delta_T$ , i.e., the time span since the last plume detection, is recorded. If  $\delta_T$  exceeds the specified threshold (i.e.,  $T_{h-max}$ ), the AUV switches to the vertical search mode, in which the AUV gradually dives and finds plumes in the vertical direction. The maximal plume non-detection period in the vertical search is defined as  $T_{v-max}$ , and if  $\delta_T$  is beyond  $T_{v-max}$ , the AUV turns to the horizontal

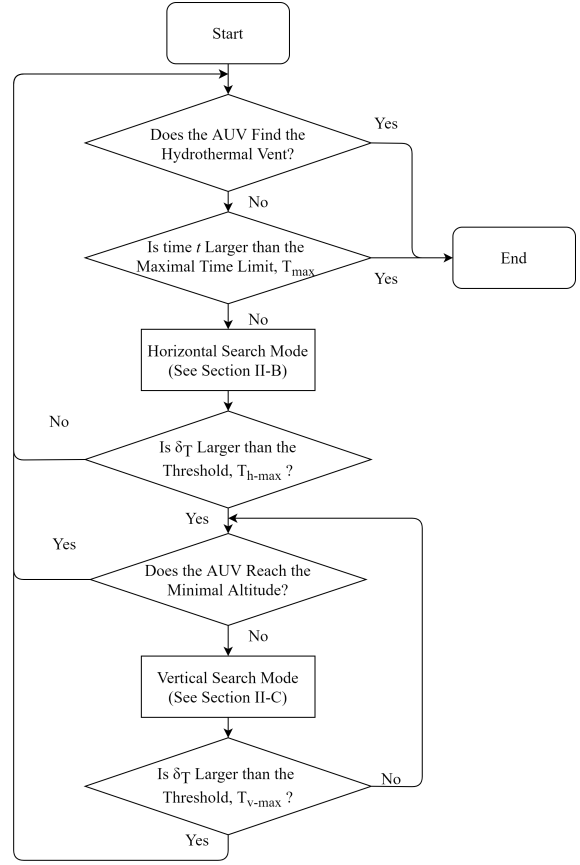


Fig. 2. The framework of the proposed CPT algorithm, where  $\delta_T$  is the plume non-detection period.

search. Once the vertical search mode is activated, the AUV altitude is monitored: when the AUV reaches the minimal altitude, it switches to the horizontal search. If the AUV finds the hydrothermal vent within the maximal time limit (i.e.,  $T_{max}$ ), the hydrothermal vent localization is treated as complete; otherwise, the localization task is terminated and the AUV returns to the initial position.

In this study, it is assumed that the AUV is equipped with a chemical sensor, a water flow sensor, and a positioning sensor, which measure local hydrothermal plume concentrations, local water flow velocities, and the AUV positions. A concentration threshold is employed to determine the plume detection events, i.e., when the sensed concentration is higher than the threshold, plumes are detected by the AUV. The hydrothermal vent is considered as being found once the AUV enters the vicinity of the source location, in which the onboard cameras could capture images and recognize the shape of a hydrothermal vent from a close distance.

### B. Horizontal Search Mode

The objective of the horizontal search mode is to find the front boundary of the plume distribution in a horizontal plane. Due to the simplicity and the light computational demand, the moth-inspired CPT method [11] is employed in the horizontal

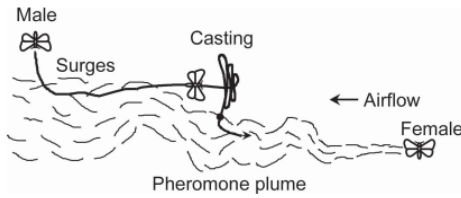


Fig. 3. A male moth traces a female moth through pheromone plumes using the 'surge/casting' behavior model. Retrieved from [23].

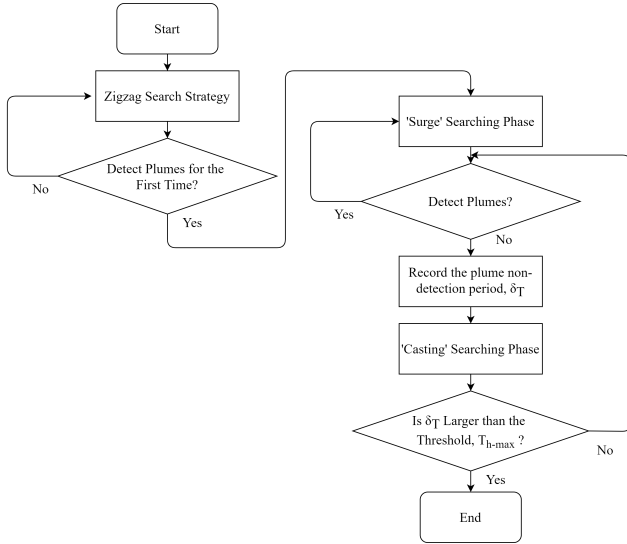


Fig. 4. The flow diagram of procedures in the horizontal search mode

search mode, which guides the AUV to trace hydrothermal plumes on horizontal planes.

The core idea of the moth-inspired CPT method is to command the robot imitating the mate-seeking behaviors of male moths, which can be summarized as a two-phase searching strategy, which comprises 'surge' and 'casting' searching phases. As shown in Fig. 3, when the male moth senses pheromone plumes emitted from the female moth, the 'surge' phase is activated and the male moth flies against the wind direction to stay inside pheromone plumes. If the male moth flies out of the plumes, it switches to the 'casting' phase, in which the male moth traverses the wind direction to re-detect plumes, and once pheromone plumes are detected by the male moth, it switches back to the 'surge' phase. The 'surge' and 'casting' phases are repeated until the female moth is located by the male moth.

We adapt the 'surge/casting' behavior model to guide the AUV in the horizontal search mode. Fig. 4 presents the flow diagram of searching procedures in this search mode. At the beginning, the AUV adopts the 'zigzag' searching trajectory [11] to sense the existence of plumes, and after the AUV detects plumes for the first time, the moth-inspired CPT strategy is activated. To implement the 'surge/casting' behavior model on an AUV, we command the AUV to move against the water flow direction when it detects plumes (i.e.,

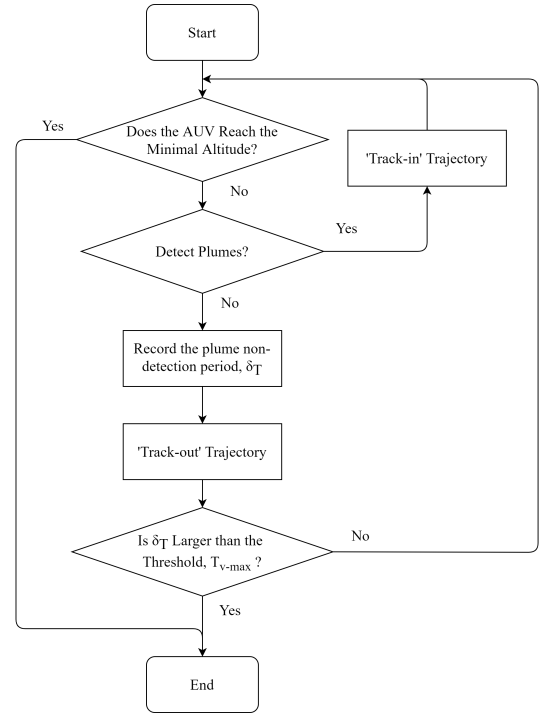


Fig. 5. The flow diagram of procedures in the vertical search mode

'surge' searching phase), and if the AUV is out of plumes, it moves in circles to re-detect plumes (i.e., 'casting' searching phase). Meanwhile, the plume non-detection period (i.e.,  $\delta_T$ ) is recorded during the 'casting' searching phase, and if  $\delta_T$  is greater than  $T_{h-max}$  (i.e., the maximal non-plume detection period in horizontal searches), the AUV switches to the vertical search mode and deactivates the current horizontal search.

### C. Vertical Search Mode

The vertical search mode is activated when the AUV has not detected plumes for a long time in the previous horizontal search mode, and its objective is to find plumes in the deeper water regions.

Fig. 5 presents the flow diagram of procedures in the vertical search mode. To avoid the AUV colliding with the seafloor while diving, AUV altitudes are monitored in vertical searches, and if the AUV reaches the minimal altitude, the current vertical search is terminated; otherwise, the AUV continues diving into deeper water regions.

Inspired by the aforementioned 'surge/casting' behavior model in the moth-inspired CPT strategy, two types of search trajectories are designed, namely 'track-in' and 'track-out' trajectories. The 'track-in' trajectory is activated when the AUV detects plumes, which is a 3-D spiral trajectory with a fixed radius, and the 'track-out' trajectory is triggered when plumes are not detected, while the AUV follows an increasing radius 3-D spiral trajectory to expand the coverage of the searching space. Besides, when the AUV is in the 'track-out' trajectory, the plume non-detection period (i.e.,  $\delta_T$ ) is recorded, and if  $\delta_T$  is larger than the specified threshold (i.e.,

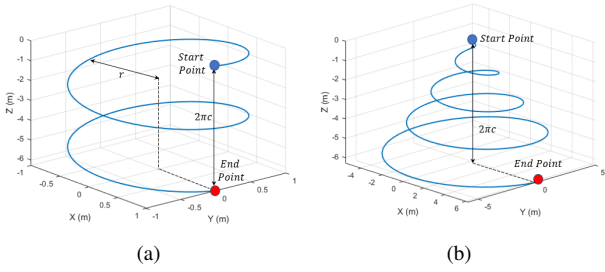


Fig. 6. (a) The plot of a sample 'track-in' trajectory, where  $(X_{start}, Y_{start}, Z_{start}) = (1, 0, 0)$ ,  $r = 1$ ,  $c = 1$  and  $a = 2$ . The start and end points of the spiral are indicated with the blue and red colors, respectively. (b) The plot of a sample 'track-out' trajectory, where  $(X_{start}, Y_{start}, Z_{start}) = (0, 0, 0)$ ,  $c = 1$ , and  $a = 4$ .

$T_{v-max}$ ), the AUV switches back to the horizontal search mode and terminates the current vertical search.

1) *'Track-in' Trajectory*: The 'track-in' trajectory is activated when the AUV detects plumes in the vertical search mode.

Inspired by the 'surge' behavior in the moth-inspired CPT method, when the AUV detects plumes in the vertical search, it is expected to maintain horizontal positions (i.e.,  $X$  and  $Y$ ) while sinking into deeper water regions. Diving perpendicularly is a possible approach (i.e., the AUV horizontal position is unchanged), but it demands a high maneuverability of AUVs (some AUVs could not move vertically), and the rapid water pressure shift may cause AUV mechanical failures. Thus, a fixed radius 3-D spiral is designed as the 'track-in' trajectory, which allows the AUV to gradually dive without significantly changing horizontal positions. Starting from a basic 3-D spiral trajectory, we derive the formula of the 'track-in' trajectory.

The basic 3-D spiral trajectory is presented as:

$$\begin{cases} x = r \times \cos(a \cdot t) \\ y = r \times \sin(a \cdot t) \\ z = c \times t \end{cases}, \quad (1)$$

where  $x$ ,  $y$ , and  $z$  are positions on the spiral,  $r$  is the radius of the spiral,  $t \in [0, 2\pi]$ ,  $c$  determines the height between the start and end points of the spiral, and  $a$  is a coefficient that determines the density of circles in the spiral: the larger the value is, the higher density of circles will be. Based on Eqn. 1, the 'track-in' trajectory can be presented as:

$$\begin{cases} x = X_{start} + r \times \cos(a \cdot t) - r \\ y = Y_{start} + r \times \sin(a \cdot t) \\ z = Z_{start} - c \times t \end{cases}, \quad (2)$$

where  $X_{start}$ ,  $Y_{start}$ , and  $Z_{start}$  are coordinates of the AUV start position in the spiral trajectories. Notice that, in order to let the AUV dive into deeper water regions,  $z$  in Eqn 1 is inverted before adding to the AUV start position. An example 'track-in' trajectory is presented in Fig. 6(a), where  $(X_{start}, Y_{start}, Z_{start}) = (1, 0, 0)$ ,  $r = 1$ ,  $c = 1$ , and  $a = 2$ .

2) *'Track-out' Trajectory*: The 'track-out' trajectory is triggered when the AUV fails to detect plumes over a period of time in the vertical search mode.

The objective of the 'track-out' trajectory is guiding the AUV to re-detect plumes in the vertical search mode. Inspired by the 'casing' behavior in the moth-inspired CPT method, we design an increasing radius 3-D spiral as the 'track-out' trajectory to enlarge the AUV exploration areas and to increase the probability of re-detecting plumes. Formulas of the 'track-out' trajectory can be presented as:

$$\begin{cases} x = X_{start} + t \times \cos(a \cdot t) \\ y = Y_{start} + t \times \sin(a \cdot t) \\ z = -Z_{start} - c \times t \end{cases}. \quad (3)$$

Note that, since the spiral radius is a variable, the fixed radius  $r$  in the basic 3-D spiral is removed. Fig. 6(b) shows the plot of a sample 'track-out' trajectory, where  $(X_{start}, Y_{start}, Z_{start}) = (0, 0, 0)$ ,  $a = 4$ , and  $c = 1$ .

When the AUV is in the 'track-out' trajectory, the plume non-detection period (i.e.,  $\delta_T$ ) is recorded. If  $\delta_T > T_{v-max}$ , the AUV switches to the horizontal search mode; otherwise, AUV remains in the vertical search mode and repeats 'track-in' and 'track-out' trajectories until reaching the minimal altitude. Besides, it is worth mentioning that the AUV altitude is a critical variable in the vertical search mode. To avoid the AUV colliding with the seafloor, AUV altitudes are monitored before performing either 'track-in' and 'track-out' trajectories, and if the AUV reaches the minimal altitude, the current vertical search is completed.

### III. EXPERIMENT AND RESULTS

#### A. The Simulation Platform

In this work, a 3-D hydrothermal plume model that imitates the realistic propagation of hydrothermal plumes is employed as the test environment. The plume model used in the simulator was designed based on a 26-month survey, which observes hydrothermal plumes in the Endeavour segment of the Juan de Fuca ridge via image sonars, conducted by the Applied Physics Laboratory at the university of Washington [24].

As shown in Fig. 7, which presents snapshots of plume distributions generated in the simulator at different time steps, the dimension of the search space is  $100 \times 100 \times 70 \text{ m}^3$ , where the  $X$  and  $Y$  axes are ranging from  $-50 \text{ m}$  to  $50 \text{ m}$  and the  $Z$  axis is from  $-1430 \text{ m}$  to  $-1500 \text{ m}$  ( $Z = 0 \text{ m}$  is the water surface). In the simulation, the hydrothermal vent is located at  $(0, -30, -1500) \text{ m}$ , and the main water flow direction is aligned with the positive direction of the  $Y$  axis. To simplify the problem, the AUV moves in a constant speed, i.e.,  $1 \text{ m/s}$ . Besides, comparing to the large scale of the search space, the size of the AUV is negligible; thus, the AUV is approximated as a single point in the simulation environment. The localization task is treated as complete if the AUV enters the surrounding region of the hydrothermal vent (i.e., the distance from the AUV to the hydrothermal vent is less than  $10 \text{ m}$ ).

#### B. A Sample Trial

This section presents results of implementing the proposed CPT algorithm in a sample trial. Values of parameters used in 3-D spiral trajectories are presented in Table I.

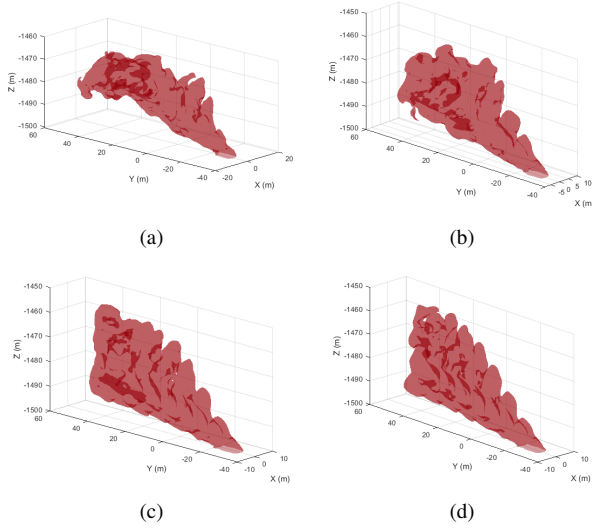


Fig. 7. A simulated hydrothermal plume at (a) 10 minutes, (b) 20 minutes, (c) 40 minutes, and (d) 60 minutes after the moment when the plume reaches a quasi-steady state. The source is located at  $(0, -30, -1500)$  m, and the plume is painted with red color to demonstrate plume distributions, while the darker color represents the higher plume concentration.

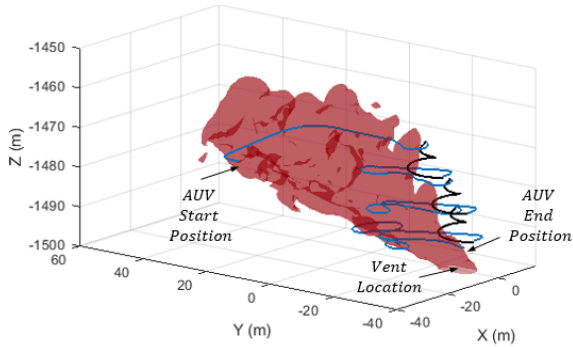


Fig. 8. The overall searching trajectory in a sample trial, where the AUV starts at the position  $(-40, 10, -1470)$  m and ends at  $(1.21, -28.44, -1495)$  m, which is very close (5.38 m) to the hydrothermal vent location, i.e.,  $(0, -30, -1500)$  m. To distinguish horizontal and vertical search modes, horizontal searching trajectories are painted with the blue color, while the vertical searching trajectories are painted with the black color.

Fig. 8 presents the overall searching trajectory in the sample trial. The minimal altitude that the AUV could reach is  $-1495$  m (i.e., five meters above the bottom). The AUV starts at  $(-40, 10, -1470)$  m and ends at  $(1.21, -28.44, -1495)$  m, which is very close (5.38 m) to the actual hydrothermal vent location, i.e.,  $(0, -30, -1500)$  m. To better demonstrate the searching trajectory in the sample trial, it is split into four sections, while each section is a combination of a horizontal search and a vertical search. Fig. 9 presents snapshots of trajectories in each section from a 3-D view and a top view.

As shown in Fig. 9(a) and Fig. 9(b), the AUV starts at the horizontal plane  $Z = -1470$  m and performs the 'zigzag' search trajectory. After it detects the plume for the first time in this plane, the AUV surges against the water flow until the plume is absent. Then, it performs the 'casting' behavior

TABLE I  
PARAMETERS USED IN THE SIMULATION AND THE CORRESPONDING VALUES

Parameter Name	Parameter Value
Fixed radius of 'track-in' trajectory (m), $r$	1
Coefficient of the spiral height, $c$	1.5
Coefficient of the circle density in the spiral, $a$	2
Maximal plume non-detection period in horizontal searches (s), $T_{h-max}$	15
Maximal plume non-detection period in vertical searches (s), $T_{v-max}$	15
Maximal time limit for a localization task (s), $T_{max}$	600
Minimal altitude that the AUV could reach (m)	-1495

by moving in circles to re-detect the plume. Since the plume non-detection period (i.e.,  $\delta_T$ ) exceeds the specified threshold ( $T_{h-max}$ ), the AUV stops the current horizontal search and conducts the vertical search. In the vertical search, the 'track-out' trajectory is activated since the AUV fails to detect the plume, and after  $\delta_T$  is greater than  $T_{v-max}$ , the AUV switches to a new horizontal search.

The second horizontal search is conducted at the plane  $Z = -1478.8$  m. Similar to the previous horizontal search, the AUV first adopts the 'zigzag' search trajectory to detect the existence of plume signals, and after the first plume detection, it surges against the flow. When  $\delta_T$  exceeds  $T_{h-max}$ , the second vertical search is activated. Due to the absence of plume detection, the AUV follows the 'track-out' trajectory in this vertical search and switches to the horizontal search when  $\delta_T$  is beyond  $T_{v-max}$ . Next, the new horizontal search is performed at the layer  $Z = -1486$  m (see Fig. 9(e)), and the subsequent vertical search brings the AUV to the next horizontal plane  $Z = -1495$  m, which is the minimal altitude that the AUV could reach. In this horizontal plane, the AUV performs moth-inspired CPT strategy to trace plumes until the hydrothermal vent is located. Finally, the AUV correctly locates the hydrothermal vent and successfully completes the localization task.

### C. Tests with Varying AUV Initial Positions

To demonstrate the validity of the proposed method in different search conditions, three more tests are conducted. In these tests, the AUV starts the hydrothermal vent localization task at varying positions. Fig. 10 presents the overall searching trajectories of these tests, namely Test 1, Test 2, and Test 3., and Table II shows the corresponding searching results. The searching trajectory of Test 1 is presented in Fig 10(a), where the AUV starts at a very high horizontal plane ( $Z = -1449$  m). In this test, six horizontal searches and five vertical searches are conducted, and the AUV successfully finds the hydrothermal vent at the location  $(1.5, -28.45, -1495)$  m in the last horizontal search.

In Test 2, the AUV starts at a horizontal plane with the middle altitude ( $Z = -1480$  m), and as presented in Fig.

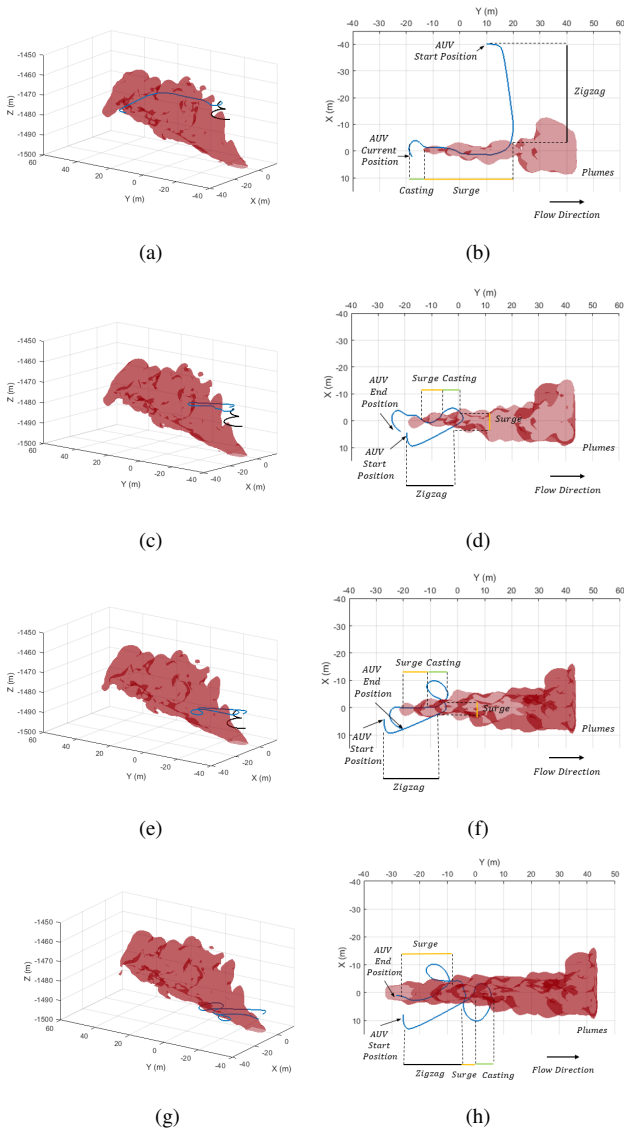


Fig. 9. Split the overall search trajectory into four sections, while each section contains a horizontal and a vertical search, and present them from the 3-D view (i.e., (a), (c), (e), and (g)) and the top view (i.e., (b), (d), (f), and (h)). In 3-D views of trajectories, the horizontal search is painted with the blue color, and the vertical search is painted with the black color. Four horizontal searches are conducted while the moth-inspired CPT strategy is implemented on the AUV. On the top view trajectories, durations of searching phases are painted with different color bars, where the black, yellow, and green color bars represent the 'zigzag', 'surge', and 'casting' phases, respectively.

10(b), after three horizontal and two vertical searches, the AUV correctly finds the hydrothermal vent at the location  $(-1.04, -29.39, -1495)$  m. In Test 3, the AUV initiates at a horizontal plane with the low altitude ( $Z = -1490$  m). There are two horizontal searches and one vertical search performed in this test. At the end of the localization task, the AUV completes the task at the location  $(-1.68, -29.86, -1495)$  m, which is in the vicinity of the hydrothermal vent. Results of these tests demonstrate the effectiveness of the proposed CPT method with varying initial positions.

It is worth mentioning that due to the lack of plume

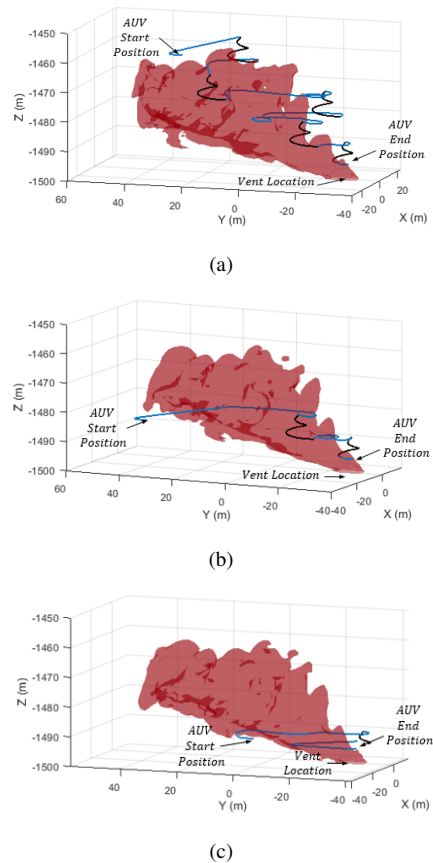


Fig. 10. Searching trajectories with the varying AUV initial positions, namely (a)  $(-30, 20, -1449)$  m, (b)  $(-40, 30, -1480)$  m, and (c)  $(-20, 0, -1490)$  m. AUV start and positions are labeled, and the horizontal and vertical searches are painted with the blue and black colors, respectively.

TABLE II  
TEST RESULTS WITH VARYING AUV INITIAL POSITIONS

Test Name	Initial Plane	Distance from the AUV to the vent (m)	Test Result
Test 1	High altitude, $Z = -1440$ m	5.44	Success
Test 2	Middle altitude, $Z = -1480$ m	5.14	Success
Test 3	Low altitude, $Z = -1490$ m	5.27	Success

distribution data in more extreme flow environments, we have not tested our method in highly turbulent flow environments. It is expected that the performance of the proposed method will not be as good as that in the laminar flow environments since the performance of the moth-inspired method employed in horizontal searches are not ideal in highly turbulent flow environments. As the alternative, the engineering-based method, such as Bayesian-inference method [12], is more efficient in turbulent flow environments.

#### IV. CONCLUSION

In this work, we propose a 3-D CPT algorithm for using on AUVs to locate a hydrothermal vent via tracing hydrothermal plumes. During the plume tracing process, two search modes,

namely horizontal and vertical search modes, are defined, while the AUV performs the moth-inspired and 3-D spiral trajectories in these two search modes, respectively. Before the AUV reaches the minimal altitude, it alternates between these two search modes depending on the plume non-detection period, which measures the time span since the last plume detection. A realistic hydrothermal plume model is employed as the simulation environment, where multiple tests are conducted with the varying AUV initial locations. Simulation results show that the proposed method is effective for finding hydrothermal vents in a 3-D underwater environment.

## REFERENCES

- [1] G. W. Luther, T. F. Rozan, M. Taillefert, D. B. Nuzzio, C. Di Meo, T. M. Shank, R. A. Lutz, and S. C. Cary, "Chemical speciation drives hydrothermal vent ecology," *Nature*, vol. 410, no. 6830, pp. 813–816, 2001.
- [2] C. R. German and J. Lin, "The thermal structure of the oceanic crust, ridge-spreading and hydrothermal circulation: How well do we understand their inter-connections," *Mid-Ocean Ridges: Hydrothermal Interactions Between the Lithosphere and Oceans, Geophys. Monogr. Ser.*, vol. 148, pp. 1–18, 2004.
- [3] C. German, L. Parson, H. Bougault, D. Coller, M. Critchley, A. Dapigny, C. Day, D. Eardley, A. Fearn, C. Flewellen *et al.*, "Hydrothermal exploration near the azores triple junction: tectonic control of venting at slow-spreading ridges?" *Earth and Planetary Science Letters*, vol. 138, no. 1-4, pp. 93–104, 1996.
- [4] J. Yuh, G. Marani, and D. R. Blidberg, "Applications of marine robotic vehicles," *Intelligent service robotics*, vol. 4, no. 4, p. 221, 2011.
- [5] G. Ferri, M. V. Jakuba, and D. R. Yoerger, "A novel trigger-based method for hydrothermal vents prospecting using an autonomous underwater robot," *Autonomous Robots*, vol. 29, no. 1, pp. 67–83, 2010.
- [6] D. S. Kelley, J. A. Karson, G. L. Früh-Green, D. R. Yoerger, T. M. Shank, D. A. Butterfield, J. M. Hayes, M. O. Schrenk, E. J. Olson, G. Proskurowski *et al.*, "A serpentinite-hosted ecosystem: the lost city hydrothermal field," *Science*, vol. 307, no. 5714, pp. 1428–1434, 2005.
- [7] S. Pang, "Plume source localization for auv based autonomous hydrothermal vent discovery," in *OCEANS 2010 MTS/IEEE SEATTLE*. IEEE, 2010, pp. 1–8.
- [8] J. A. Farrell, J. Murlis, X. Long, W. Li, and R. T. Cardé, "Filament-based atmospheric dispersion model to achieve short time-scale structure of odor plumes," *Environmental fluid mechanics*, vol. 2, no. 1-2, pp. 143–169, 2002.
- [9] H. Ishida, K.-i. Suetsugu, T. Nakamoto, and T. Moriizumi, "Study of autonomous mobile sensing system for localization of odor source using gas sensors and anemometric sensors," *Sensors and Actuators A: Physical*, vol. 45, no. 2, pp. 153–157, 1994.
- [10] R. T. Cardé and M. A. Willis, "Navigational strategies used by insects to find distant, wind-borne sources of odor," *Journal of chemical ecology*, vol. 34, no. 7, pp. 854–866, 2008.
- [11] W. Li, J. A. Farrell, S. Pang, and R. M. Arrieta, "Moth-inspired chemical plume tracing on an autonomous underwater vehicle," *IEEE Transactions on Robotics*, vol. 22, no. 2, pp. 292–307, 2006.
- [12] S. Pang and J. A. Farrell, "Chemical plume source localization," *IEEE Transactions on Systems, Man, and Cybernetics, Part B (Cybernetics)*, vol. 36, no. 5, pp. 1068–1080, 2006.
- [13] J.-G. Li, Q.-H. Meng, Y. Wang, and M. Zeng, "Odor source localization using a mobile robot in outdoor airflow environments with a particle filter algorithm," *Autonomous Robots*, vol. 30, no. 3, pp. 281–292, 2011.
- [14] J. A. Farrell, S. Pang, and W. Li, "Plume mapping via hidden Markov methods," *IEEE Transactions on Systems, Man, and Cybernetics, Part B (Cybernetics)*, vol. 33, no. 6, pp. 850–863, 2003.
- [15] Z. A. Saigol, R. W. Dearden, J. L. Wyatt, and B. J. Murton, "Information-lookahead planning for auv mapping," in *Twenty-First International Joint Conference on Artificial Intelligence*, 2009.
- [16] H.-f. Jiu, S. Pang, J.-l. Li, and B. Han, "Odor plume source localization with a pioneer 3 mobile robot in an indoor airflow environment," in *IEEE SOUTHEASTCON 2014*. IEEE, 2014, pp. 1–6.
- [17] L. Wang and S. Pang, "Chemical plume tracing using an auv based on pomdp source mapping and a-star path planning," in *OCEANS 2019 MTS/IEEE SEATTLE*. IEEE, 2019, pp. 1–7.
- [18] M. Vergassola, E. Villermaux, and B. I. Shraiman, "'infotaxis' as a strategy for searching without gradients," *Nature*, vol. 445, no. 7126, p. 406, 2007.
- [19] J. A. Farrell, S. Pang, and W. Li, "Chemical plume tracing via an autonomous underwater vehicle," *IEEE Journal of Oceanic Engineering*, vol. 30, no. 2, pp. 428–442, 2005.
- [20] G. Ferri, M. V. Jakuba, A. Mondini, V. Mattoli, B. Mazzolai, D. R. Yoerger, and P. Dario, "Mapping multiple gas/odor sources in an uncontrolled indoor environment using a bayesian occupancy grid mapping based method," *Robotics and Autonomous Systems*, vol. 59, no. 11, pp. 988–1000, 2011.
- [21] H. Hu, S. Song, and C. P. Chen, "Plume tracing via model-free reinforcement learning method," *IEEE transactions on neural networks and learning systems*, 2019.
- [22] H. Jiu, Y. Chen, W. Deng, and S. Pang, "Underwater chemical plume tracing based on partially observable markov decision process," *International Journal of Advanced Robotic Systems*, vol. 16, no. 2, 2019. [Online]. Available: <https://doi.org/10.1177/1729881419831874>
- [23] H. Ishida, Y. Wada, and H. Matsukura, "Chemical sensing in robotic applications: A review," *IEEE Sensors Journal*, vol. 12, no. 11, pp. 3163–3173, 2012.
- [24] J. Lavelle, D. Di Iorio, and P. Rona, "A turbulent convection model with an observational context for a deep-sea hydrothermal plume in a time-variable cross flow," *Journal of Geophysical Research: Oceans*, vol. 118, no. 11, pp. 6145–6160, 2013.